Received: Januari 2026	Accepted: April 2025	Published: April 2025

Comparative Evaluation of Gradient Operators with Otsu Thresholding for Microscopic Porosity Detection

Himawan Wicaksono[1*], Alamsyah[2], Suardi[2], Muhammad Malikul Mulki[2]

[1]Electrical Engineering Study Program, Department of Electrical Engineering, Informatics, and Business, Kalimantan Institute of Technology

[2]Naval Architecture Study Program, Department of Maritime Technology, Kalimantan Institute of Technology

[*]Email: himawan@lecturer.itk.ac.id

Abstract

This study demonstrates the comparison of five well-known gradient operators —Sobel, Prewitt, Roberts, Scharr, and Laplacian of Gaussian (LoG)—using the classical technique of Otsu thresholding to detect microscopic porosities in SMAW welds of ship structures. This was done using 33 images of micrographs taken at 25x magnification, with all images preprocessed using standardization techniques (grayscale conversion, Gaussian filtering, and normalization), and the results were compared using six different performance evaluation criteria —Precision, Recall, F-Measure, Peak Signal-to-Noise Ratio (PSNR), Edge Co-occurrence Matrix (ECM), and Matthews Correlation Coefficient (MCC). The results indicate that the Sobel operator produced the largest PSNR value (≈42.5 dB) indicating that the Sobel operator provided the greatest fidelity in image quality. Additionally, the Scharr operator had the largest MCC (0.94) and ECM correlation (0.99), indicating that it provided the greatest reliability and coherence in texture. The Roberts operator produced the largest F-measure (0.23), indicating that it provided a good balance between the two evaluation metrics. In summary, the Scharr operator demonstrated the most consistent and interpretable performance among the three performance evaluation metrics, providing both the best visual fidelity and structural texture stability. Therefore, the proposed methodology represents a reproducible and computationally efficient reference for automated microscopic inspections and smart NDT in maritime welding applications.

Keywords: Microscopic Porosity, Gradient Operators, Otsu Thresholding, Edge Detection Metrics, SMAW Welds.

1. Introduction

Ship construction relies heavily upon welds. The welds themselves make up a large part of a ship's structure. Therefore, if there are any problems with welds, it will negatively affect how well a ship performs. Porosity is one problem that is significant because it is formed when bubbles form inside of the metal as it cools down after being welded. This creates weak points in the metal that can cause failure faster than other types of failures, including those caused by corrosion and fatigue.

Because weld quality is becoming so important for ensuring ship safety, and because porosity can be difficult to detect visually, microscopic analysis has been used to detect porosity at the micro-level. A number of researchers have shown that porosity causes fatigue in ship steel [1][2][3], and several of them have also demonstrated that the size and location of pores play an important role in determining fatigue life [1][2][3]. In fact, these researchers found that even small pores can serve as locations where stresses concentrate. Researchers also found that the existing standards for evaluating the reliability of welds based on porosity may underestimate the long-term fatigue reliability of welds containing pore clusters [3].

Clearly, a method for efficiently and accurately detecting porosity at the micro-level needs to be developed to improve weld quality and safety. Non-destructive testing (NDT) is a valuable tool for detecting defects in materials. NDT includes methods such as ultrasonic testing, radiographic testing, and liquid penetrant testing. While these methods are excellent tools for detecting defects larger than the wavelength of the test method and surface cracks, they are poor at detecting subsurface defects such as micro-pores. Digital microscopic imaging has therefore emerged as a necessary tool for detecting defects in welds that cannot be seen with the naked eye. Digital microscopic imaging allows researchers to collect detailed, high-resolution images of the defects in a weld, and use this information to develop more effective ways to evaluate weld quality.

The characteristics of the weld defect known as porosity are determined by many factors, both metallurgically related to the base material and process related to the weld itself. For example, the heat input, current, and cooling rates all influence the size, shape, and distribution of pores in a weld [4-5]. Because the characteristics of porosity are influenced by a variety of different factors, developing automated methods to identify porosity in images obtained through digital microscopic imaging is very complex.

The difficulty lies in the ability of computer algorithms to isolate the areas of porosity from the surrounding areas of metal. In addition to the difficulty of isolating the areas of porosity, the presence of illumination variations and background noise makes the task of identifying porosity very complex. Additionally, the complexity of the image, due to the varied texture of the metallic surface, adds to the difficulty of segmenting the images into distinct areas of porosity and metal.

Gradient methods are used as an analytical tool to identify intensity discontinuities between pixels to create a boundary of defects. Methods include classical gradient methods – Sobel, Prewitt, Roberts, Scharr, and Laplacian of Gaussian (LoG), which calculate the directional derivative to emphasize structural differences within an image; and these can be utilized with adaptive thresholding, such as Otsu's method, to allow automatic separation of object regions from background thereby enhancing defect visualization.

The robustness of classical gradient methods has been demonstrated through multiple studies in both image processing and materials science: Liu et al., [4] illustrated the superiority of the Scharr operator under conditions of weak edges; while [5] demonstrated the higher frequency noise tolerance of the Scharr operator. In addition to classical gradient methods, deep learning methods have also shown effectiveness for the detection of defects in welds. For example, Zhang et al., [6] implemented a CNN based approach that yielded high accuracy for the detection of macro-defects in radiographic weld images; while Hoa et al. [7] introduced Weld-CNN, a hybrid model that combined convolutional and edge-based feature extraction. While both methods are successful, there is still a need for them to utilize large datasets, and they provide little in terms of interpretability; whereas classical gradient-based methods are beneficial due to their simplicity, low computational costs and physical interpretability, providing advantages over deep learning methods when utilizing real time industrial inspection systems.

Several studies have examined edge detection, however there remains a methodological gap in the literature; very few studies have compared the performance of classical gradient operators for detecting microscopic porosity in SMAW welds. Most studies that have provided comparisons among gradient operators were restricted to biomedical and/or medical imaging [8]; therefore, limited validation was available for use in industrial metallographic applications.

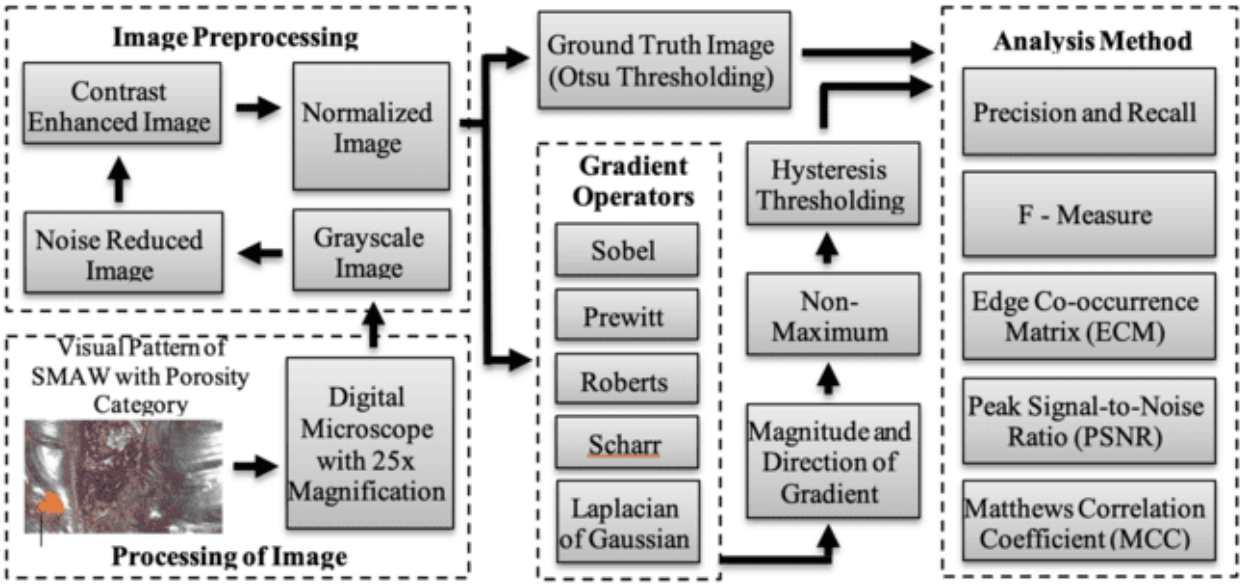

Figure 1. Flow diagram of edge detection process based on gradient operators and analysis methods

This study addressed this gap by comparing the performance of five gradient operators – Sobel, Prewitt, Roberts, Scharr, and LoG – using Otsu's method for adaptive thresholding to detect microscopic porosity in SMAW welds.

This paper utilizes numerous quantitative evaluation metrics—precision, recall, f-measure, peak signal-to-noise ratio (PSNR), edge co-occurrence matrix (ECM) and Matthews correlation coefficient (MCC)—to provide a comprehensive assessment of operator detection accuracy, the quality of visually generated images, and texture stability.

The data set utilized was the Microscopic Image Dataset on Visual Patterns of SMAW Results in Ship Structures with Porosity Category [9]. This data set is officially registered as part of the Ministry of Law and Human Rights (Indonesia), thus providing legal certainty and allowing for replication of the results by other researchers.

As a research project that builds upon classical gradient theory, but which applies that theory to microscopic metallurgical imaging, the study identifies the operator's ability to adapt to real world conditions of high levels of noise, uneven lighting and irregular surface topography.

As such the study provides a scientifically validated reproducible and computationally efficient foundation upon which to build automated inspection and artificial intelligence-based nondestructive testing (NDT) capabilities within ship building.

To address the existing methodological gap, this study poses the following research questions: (i) How do five classical gradient operators (Sobel, Prewitt, Roberts, Scharr, and LoG) perform comparatively in detecting microscopic porosity edges in SMAW welds? (ii) Which operator provides the optimal balance between visual detection accuracy and structural texture stability?

The main contributions of this research are twofold: first, benchmarking classical gradient operators under standardized industrial microscopic conditions to establish a performance reference; and second, providing a computationally efficient and validated edge-detection framework that can serve as a foundation for intelligent, AI-based Non-Destructive Testing (NDT) systems in shipbuilding.

To achieve this, the evaluation methodology utilizes Otsu thresholding as a reference baseline to segment the weld

porosity. The performance of each gradient operator is then quantitatively summarized and compared using six metrics: Precision, Recall, and F-Measure for detection accuracy; Peak Signal-to-Noise Ratio (PSNR) for visual fidelity; Matthews Correlation Coefficient (MCC) for classification reliability; and the Edge Co-occurrence Matrix (ECM) for texture stability.

2. Method

2.1 Research Design

Using an experimental - comparative methodology, this research evaluates the performances of five traditional gradient operators (Sobel, Prewitt, Roberts, Scharr, and LoG) on the detection of microscopic porosity in shielded metal arc welding (SMAW) welds from ship construction (see Figure 1). All five operators were used identically after similar pre-processing and thresholding to provide for objective comparisons among the different operators. Edge detection through gradient methods has been the basis of much of the early development in digital image processing because it is easy to understand and relatively inexpensive computationally.

To allow for comparability between the results obtained with each gradient operator, Otsu's thresholding was selected as a base line comparator which maximizes interclass variance to separate objects of interest from the background. Therefore, this research utilizes a comprehensive framework integrating traditional gradient operators with adaptive thresholding to provide reproducible and efficient porosity detection.

Performance comparisons of the different gradient operators are quantitatively assessed using six parameters: Precision, Recall, F-Measure, Edge Co-occurrence matrix (ECM), Peak Signal to Noise Ratio (PSNR), and Matthews correlation coefficient (MCC); these parameters provide a balanced measure of accuracy, robustness, and interpretability for the evaluation of SMAW weld porosity.

2.2 Research Duration and Locations

During the experimentation phase the study was performed during a time span of approximately 4 months, February – May 2025 and in two different laboratory settings ― both in an industrial environment and within an educational setting ― as a way to provide a high level of authenticity in terms of how welding operations are performed in real-world applications and simultaneously to obtain high levels of analytical precision.

Industrial Setting (Shipyard, Pontoon Repair Yard Balikpapan, East Kalimantan).

During the field phase of this study, the research was conducted at a shipyard and pontoon repair facility located in Balikpapan, Indonesia; allowing researchers to obtain access to actual SMAW welded structures and their associated porosity due to the various factors related to environmental and operational variability which occur when welding is performed on marine structural components. Image acquisition using CCD cameras in the field provides a means of obtaining algorithms that can be resilient to all types of illumination noise, surface contamination, and spatial irregularities that may occur in field environments.

Field vs. Laboratory Context of Study

The two context levels in this study are a laboratory setting at ITK's Computer Vision Laboratory, which is an environment where all aspects of processing and analysis can be controlled and standardized to allow for the same level of preprocessing of all images and quantitatively evaluate each image processed by a given operator. Microscopic images from the field site were standardized by resolution, illumination and normalized to have the same gray scale as the others to enable a fair comparison between operators. Gouda et al. [14] and Kim and Min [15] have also emphasized the importance of combining field and laboratory data to achieve higher levels of reproducibility in analysis and clarity in interpretation.

Ecological Validity & Analytical Rigor

This study achieves ecological validity and analytical rigor through its use of both a real-world industrial environment and a highly controlled laboratory environment. A controlled laboratory provides precision and repeatability of results, while the industrial site provides the opportunity for authentic variability to be tested. This approach follows those presented by Dharmawan and Lee [16] and Jiao et al., [17] which show that the inclusion of multiple environments for acquiring data increases the applicability of models created through artificial intelligence assisted welding inspections, the accuracy of tracking defects and increases the ability of researchers to reproduce findings in the future.

2.3 Population, Sample, and Sampling Technique

In addition to being composed of microscopic images of SMAW weld joints of various ship structures; which are representative of common porosity levels found within industry, the population of this study is made up of various images used as examples of porosity (i.e., based upon the images used within the research). The population was defined by how each of the images were represented computationally for analysis purposes as opposed to the physical specimen itself having unique features such as texture, lightness, and distribution of pores.

Thirty-three images were selected using a purposeful selection process in order to ensure that all porosity types from infrequent pores on the surface of the sample to frequent, large pores inside the sample were included to allow for the widest range of variability possible between images for the comparison of algorithms. Each of the images selected originated from the legally registered dataset titled "Gambar Mikroskopik Pada Pola Visual Hasil Pengelasan SMAW Pada Struktur Kapal Dengan Kategori Porositas (Porosity)" [9]. This dataset was specifically curated to include data that was both controlled, yet relevant to the use of image-based methods to determine porosity in welds.

Due to the emphasis of the dataset being morphologically diversified as opposed to randomly representative of the population, this study employed a non-random sampling strategy termed Purposive (Non-Probability), where images that had significant pore diversity and thus provided meaningful information were intentionally selected.

In addition to those mentioned above, researchers in materials and welding have also utilized comparable purposive sampling methods. Thi Hoa et al. [18] demonstrated how variability in data sets, including porosity, cracks, and lack-of-fusion defects, contribute to the robustness of models, while Xu et al. [19] demonstrated how the intentional selection of images that contain a variety of visually complex porosity prior to processing enhances the generalizability of algorithms, regardless of the number of samples used.

All of the micrographs were captured at 25x magnification utilizing a digital microscope with a 1080-pixel horizontal resolution. Staab et al. [20] found that a consistent resolution and contrast are necessary for consistent interpretations of microstructures; therefore, the relatively low sample size (n = 33), is supported by the high level of control.

As has been shown by Das et al. [21] and Meng et al. [22], when samples are well-curated and small, they can provide reliable, replicable insights into porosity behaviors and are practical for both realistic and computational evaluations.

The study's sampling strategy represents a purposeful, image-based sampling approach which provides a strong empirical basis for examining the relative performance of gradient-operators in SMAW welds, as well as a means of detecting porosity using Otsu thresholding in an automated inspection environment.

2.4 Research Methodology

Research methodology is a clear and detailed sequence of the steps we will take in our investigation. The Research Flow Diagram (see Figure 1) shows that we will follow an eight-step sequence which demonstrates

transparent methodology, rigorous analytical techniques and reproducible findings. The flow diagram illustrates the logical sequence of each stage of the investigation ― from collecting the data to conducting the quantitative analyses ― based upon the logic of experimentation established by Wicaksono [8] and incorporates current theoretical and practical developments in the field.

2.4.1. Sampling Images

We collected microscopic images of SMAW welds from the structure of ships using a digital microscope (25x magnification, 1080 pixels per image). We sampled areas where there could be potential porosity due to surface irregularity. While this level of magnification allows sufficient pixel density for analysis at the texture level, it has been shown by Li et al. [23] and Nasibov [24] that both spatial resolution and optical calibration are important to the accurate interpretation of micro-defects in images. In line with the recommendations of Wicaksono [8], we used the 25x configuration to provide sufficient detail and control over noise while avoiding oversampling and aliasing in order to preserve spatial integrity and maintain edge fidelity in accordance with metallurgical micrograph standards.

2.4.2. Image Preprocessing

Preprocessing improved the quality, reliability, and consistency of the images prior to their use with gradient-based edge detection operators. All SMAW microscopic images were standardized to include equivalent levels of luminance and structural uniformity so that each image could be analyzed in an identical manner. The image preprocessing pipeline consisted of three steps: (i) grayscale conversion, (ii) application of Gaussian smoothing filters, and (iii) normalization of image contrast. Grayscale conversion was used to remove redundant data from color images while preserving both the structural detail and brightness within the images; (ii) Gaussian smoothing filters were applied to suppress the presence of high frequency noise without blurring the edges; and (iii) normalizing the contrast between all images provided a common reference point for comparison of luminance levels across images. Together, these preprocessing methods standardized the image dataset, thereby allowing comparisons of the performance of various edge detection algorithms to reflect their inherent characteristics rather than any variability caused by the imaging process itself.

Grayscale Conversion

To improve the efficiency of processing the images while maintaining structural and brightness details necessary for edge detection, color micrographs were converted to grayscale images. Since the primary source of edge information is the variation in brightness throughout the image, using grayscale images resulted in significant savings of computational resources. Converting color images to grayscale images utilized the standard luminance model, which can be expressed as follows:

$$I_{gray} = 0.299R + 0.587G + 0.114B \text{.....(1)}$$

In **Equation 1**, the variables R, G, and B represent the intensity values of the red, green, and blue color channels, respectively. In equation 1, the greatest weight is assigned to the value of the green color channel. This was done because it reflects the fact that the human visual system has greater sensitivity to wavelengths found in the mid-spectral range. Using the values from the original color image and applying them according to equation 1 results in a new image that has been weighted to maintain tonal balance and spatial coherence, both of which are important factors in consistently computing gradients.

As shown by Wicaksono [8], converting color images to grayscale images utilizing a luminance-weighted formula improves the coherence of edges in microscopy images of Bacillus sp., while, as demonstrated by Kakumani and Sree [27], converting color images to grayscale images utilizing a similar luminance-weighted formula provides improvements in the accuracy of segmentation in fluorescence microscopy. Therefore, this

method preserves the consistency of the preservation of the edges within the images of SMAW samples and forms a reliable base upon which to apply Gaussian denoising.

Gaussian Filtering for Noise Reduction

Following gray-scale conversion, the SMWA images were smoothed by a two-dimensional (2D) Gaussian filter to remove high-frequency noise caused by both illumination and/or sensor variability. The mathematical representation of this filter is given as follows:

$$G(x,y) = \frac{1}{2\pi\sigma^2} exp\left(-\frac{x^2+y^2}{2\sigma^2}\right) \text{.....(2)}$$

The standard deviation value (σ) determines the amount of smoothing applied. To ensure consistency and replication, a fixed value of σ = 1.2 pixels was chosen and applied identically across all images and operators. This specific value provided optimal denoising quality without over-smoothing edges or leaving small areas of noise which would reduce the accuracy of gradient magnitude measurements. Turk et al. [25] similarly combined Gaussian pre-conditioning with deep activation mapping to increase the peak signal-to-noise ratio (PSNR) and signal-to-noise ratio (SNR) for images obtained through metallography; Salwig et al. [26] have also demonstrated the utility of Gaussian prior models for photon-limited microscopy. These approaches allowed the preservation of detail at fine pore boundaries, reduction of random fluctuations in background values and thereby stabilized the orientation of the gradients for correct evaluation of edges.

Contrast Enhancement and Normalization

Following denoising, intensity normalization addressed differences in illumination (i.e., different lighting conditions) between images within the dataset and therefore normalized each image to be comparable to every other image, so that all images were equivalent. The normalization of intensity removed unevenness in brightness due to light scattering or curvature of the lens. After normalization of intensity, contrast enhancements were applied to increase the contrast of faint edges and improve the local contrast by increasing the intensity dynamic range using linear stretching as follows:

$$I_{enh} = \frac{I-I_{min}}{I_{max}-I_{min}}\ x\ 255 \text{ .....(3)}$$

Where I is the current intensity value, I_{min} is the lowest intensity value found in the image (pixel intensity), and I_{max} is the highest intensity value found in the image (pixel intensity). Following contrast enhancements, the data were z-normalized to normalize the intensity distribution for each image across all images:

$$I_{norm} = \frac{I-\mu}{\sigma} \text{ .....(4)}$$

Where I is an individual intensity value, μ is the average intensity of all pixels in the image, and σ is the standard deviation of all intensity values in the image. The z-normalizing process normalizes the histogram of the image; thus, it ensures consistent brightness and contrast among all images. Therefore, this process prevents bias in the evaluation of PSNR, MCC, and ECM metrics in subsequent analyses. Govindaraju et al. [28], illustrated the effectiveness of combining histogram corrections with deep image priors to enhance the perceptually smoothed and balanced luminance characteristics of microscopic images. As such, the intensity normalization provided stable illumination, reduced noise and normalized the contrast in the dataset to provide a statistical consistent dataset that can serve as a valid basis for the use of gradient based edge detection algorithms in SMAW porosity imaging.

2.4.3. Application of Gradient Operators

Gradient operators in five classic forms— Sobel, Prewitt, Roberts, Scharr, and LoG were used to analyze transitions in local intensity due to porosity boundary detection on SMAW images after image preprocessing. The edge-detection robustness was evaluated by comparing the results of the five operators which are sensitive to direction and resistant to

noise and then subsequently evaluating the PSNR, MCC, and ECM metric values because of quantitatively analyzing the edge-detection performance.

A. Sobel Operator

A Sobel filter is useful to enhance the transition of horizontal/vertical edges while giving more weight to the center pixel in the Sobel Convolution Filter (as well as other filters), which can be effective to remove some types of noise while also to preserve edge transitions in images that have multiple types of texture [8], [10]. The Sobel filter's two convolution matrixes are:

$$G_x = \begin{bmatrix} -1 & 0 & 1 \\ -2 & 0 & 2 \\ -1 & 0 & 1 \end{bmatrix}, \; G_y = \begin{bmatrix} 1 & 2 & 1 \\ 0 & 0 & 0 \\ -1 & -2 & -1 \end{bmatrix} \quad .....(5)$$

The magnitude and direction of the gradient are determined by:

$$G = \sqrt{G_x^2 + G_y^2}, \quad \theta = tan^{-1}\left(\frac{G_y}{G_x}\right) \quad .....(6)$$

Sobel has been found to be very effective at resisting the effects of random noise [10]; although it is even better with a Gaussian pre-filter applied to the image [10]. In addition to this, Wicaksono was able to find that Sobel produced the largest PSNR value for Bacillus sp. microscopy, thereby confirming cross-domain effectiveness for both biological and metallurgical edge detection [8]. Due to these characteristics, Sobel is used as a reference point for creating a steady progression of gradients in SMAW porosity images.

B. Prewitt Operator

The Prewitt operator has a uniform weighting of the kernels in that there is a lessened sensitivity to noise and increased efficiency in computation. The convolution matrices of the Prewitt operator are defined by:

$$P_x = \begin{bmatrix} -1 & 0 & 1 \\ -1 & 0 & 1 \\ -1 & 0 & 1 \end{bmatrix}, \; P_y = \begin{bmatrix} -1 & -1 & -1 \\ 0 & 0 & 0 \\ 1 & 1 & 1 \end{bmatrix} \quad .....(7)$$

The Prewitt operator detects moderate intensity gradient changes and transition from one uniform microtexture to another. As stated in [12], Saydazimov et al., Prewitt operator offers a good balance between sharpness and computational efficiency; thus, it can be used in real time imaging applications.

C. Roberts Operator

Using a compact 2x2 convolution mask to calculate the diagonal gradient, the Roberts operator provides an accurate location of sharp transition of the intensity (in addition to being inherently sensitive to noise).

$$R_x = \begin{bmatrix} 1 & 0 \\ 0 & -1 \end{bmatrix}, \; R_y = \begin{bmatrix} 0 & 1 \\ -1 & 0 \end{bmatrix} \quad .....(8)$$

Although the Roberts operator is inherently noise sensitive, it has been demonstrated by Wicaksono [8], that the combination of the Roberts operator calculating the diagonal gradients and applying morphological filters results in a highly effective micro defect localizer; and by Maksimovic et al., [10], that the Roberts operator can be used for adaptive thresholding. Therefore, in SMAW imaging, the Roberts operator is useful for highlighting the sharp edge of pores located in high contrast and compact regions.

D. Scharr Operator

The Scharr operator has an isotropic gradient response with rotational symmetry; this is a benefit to help minimize directionality bias of the edges and provide consistent edge strength regardless of orientation [8], [10]. The kernels for the Scharr operator are stated as:

$$S_x = \begin{bmatrix} 3 & 0 & -3 \\ 10 & 0 & -10 \\ 3 & 0 & -3 \end{bmatrix}, \; S_y = \begin{bmatrix} 3 & 10 & 3 \\ 0 & 0 & 0 \\ -3 & -10 & -3 \end{bmatrix} \quad ...(9)$$

This makes the Scharr's robustness under uneven lighting, commonly seen in metallography images possible. Wicaksono [8] found that it had the best Matthews Correlation Coefficient (MCC), indicating the most stable segmentation when classifying microstructures. Similarly, Maksimović et al. [10] were able to verify the reliability of the Scharr operator for detecting edges at multiple directions under different noise conditions.

E. Laplacian of Gaussian (LoG) Operator

The Laplacian of Gaussian (LoG) operator is a combination of the second order derivatives (second order differentiation), and Gaussian smoothing, used to reduce the presence of high frequency noise while accentuating sudden transitions in intensity [29][30].

$$\nabla^2 G(x,y) = \frac{\partial^2}{\partial x^2} + \frac{\partial^2 G}{\partial y^2} \quad \text{.....(10)}$$

The LoG operators have been successfully applied to detecting the pores edges by eliminating the unwanted background noises and emphasizing the curvatures; It is able to define the circular and irregular pore boundary. An improvement on the traditional LoG was proposed by Tang et al. [29] named ILoG (Improved LoG) for the high-noise mechanical imaging application; Alcaraz-Chavez et al. [30] proved the LoG applicability to the cytological segmentation. Therefore, the LoG is appropriate for the use of both edge precision and smoothness through the combination of Gaussian smoothing and second derivative sensitivity, so that it is suitable for the analysis of micro welds porosity and structural defects.

2.4.4. Computation of Gradient Magnitude and Direction

Using horizontal G_x and vertical G_y gradients generated by the convolutional kernels, the gradient magnitude $M(x,y)$, and the angle of orientation $\theta(x,y)$ are determined as follows:

$$M(x,y) = \sqrt{G_x^2 + G_y^2},$$
$$\theta(x,y) = tan^{-1}\left(\frac{G_y}{G_x}\right) \quad \text{.....(11)}$$

The two described parameters represent how strong the edges are in a sample and whether they are oriented along specific directions of interest in terms of describing the distribution of the porosity at the microstructure level. The determination of the correct orientation of textures in images can be critical when using metallography. Gradient orientations in the work of Wicaksono [8] were identified as being one of the primary factors responsible for maintaining consistent images across domains; Li et al. [31] have shown that optimizing gradient magnitudes and directions with adaptability improves segmentation accuracy and minimizes the effects of angular distortion under various levels of illumination and noise conditions and thus increase the reliability of the interpretation of the texture.

2.4.5. Non-Maximum Suppression (NMS)

To improve edge continuity, a non-maximum suppression (NMS) process was used to reduce redundant or weak edge detection results. Only those peaks that are in the same direction as the gradient were retained. This can be described mathematically as follows:

$$M'(x,y) = \begin{cases} M(x,y), \ if\ M(x,y) > M(p_1), M(p_2)\ along\ \theta(x,y) \\ 0, \ otherwise \end{cases} \quad \text{....(12)}$$

The function of this process was to remove redundant and/or weak edge detection results leaving sharp one pixel boundary representations. Traditional NMS algorithms generally retain overlapping edges resulting from noisy image conditions. However, the use of adaptive confidence maps and geometric suppression has resulted in better localization of edges and overall structural consistency [32]. In addition, Alcaraz-Chavez et al. [30] demonstrated higher precision and recall rates when analyzing cytology and metallography images. Wicaksono [8] previously applied NMS to enhance microscopic texture representation which will now be applied to the SMAW micro-porosity analysis.

2.4.6. Hysteresis Thresholding

After Non-Maximum Suppression (NMS) was applied, Hysteresis Thresholding was used to identify the strongest edges that were most likely true and eliminate all of the weaker responses. The use of this dual-threshold technique for the classification of a pixel as either a "strong," "weak," or "no" edge based upon its gradient value provides both continuity to edge detection and minimizes false positive results from the edge detection algorithm. Local contrast and contextual statistical-based

adaptive hysteresis models [33] are useful in the preservation of micro-level edge detail in noisy environments; this methodology is also consistent with Wicaksono's [8] research on adaptive threshold calibration to achieve an optimal balance between precision and retained edge quality within varying illumination conditions.

To guarantee experimental reproducibility, the dual thresholds for the hysteresis process were explicitly fixed for all gradient operators. The thresholds were calculated dynamically as a percentage of the maximum gradient magnitude within each specific image, set precisely at T_{high} = 0.70 x max(gradient) and T_{low} = 0.30 x max(gradient).

2.4.7. Otsu Thresholding as a Reference Baseline

Otsu's method has been utilized to create a pseudo-reference baseline to objectively separate the foreground (porosity) from the background (metal) and evaluate the gradient operators' performance. While manual annotation by metallurgical experts represents the absolute gold standard for reference baseline, manual segmentation at the microscopic level is highly susceptible to human subjectivity, fatigue, and is difficult to reproduce. Therefore, Otsu's adaptive global thresholding was selected to provide a statistically optimized, mathematically objective, and computationally reproducible baseline for comparison. It is acknowledged as a limitation of this study that the evaluation metrics primarily measure the operators' conformity to the Otsu segmentation baseline, rather than absolute conformity to a metallurgically and physically verified porosity map.

2.4.8. Data Analysis and Performance Metrics

To measure how well each of the gradient operators detected microscopic porosity, six quantitative measures were used: precision, recall, f-measure, PSNR, MCC and ECM. These are a combination of measures that assess detection accuracy as well as image quality and textural consistency in images of the micrograph. The process for evaluating each of the gradient operator's outputs is based on an extension of adaptive edge-detection and image-quality methodologies [31]. Wicaksono's [8] comparative methodology was extended to provide a basis for reproducibility and statistical consistency when comparing each of the gradient operator's output to an Reference Baseline (Otsu).

A. Precision and Recall

The Precision (P) and Recall (R) represent both the discrimination between real and false edges and the comprehensive detection of true edges by edge detectors. They can be described using the following equation.

$$P = \frac{TP}{TP+FP}\ , \quad R = \frac{TP}{TP+FN} \quad \text{.....(13)}$$

True positives (TP), false positives (FP) and false negatives (FN) are denoted by the acronyms TP, FP and FN respectively. In general, a higher precision is indicative of lower false edges while a higher recall is an indicator of a greater number of true edges detected. Maintaining this equilibrium for both avoids either under or over segmentation. Recent studies [10],[31] have shown that adaptive threshold adjustment allows to reach a better precision-recall equilibrium for complex microscopic images than other approaches; these findings support the results of Wicaksono [8], who demonstrated that an optimal balance provides a faithful representation of the porosity-boundary throughout biological and metallurgical micrographs.

B. F-Measure (Harmonic Mean of Precision and Recall)

In order to combine both metrics into one unified metric, the F-Measure, also known as the F1-Score, can be determined by using the following formula:

$$F_1 = 2\ x\ \frac{P\ x\ R}{P+R} \quad \text{.....(14)}$$

As the harmonic mean of precision and recall, the F-Measure (F_1) will help determine how imbalanced those two are toward each other in addition to serving as an indicator of the reliability of edge detection. Studies have shown that higher F_1 values indicate more sharply defined and localized edges [34]. In the area of metallographic imaging, a balanced F_1 value will provide accurate pore identification while avoiding the exaggeration of false positive edge detection for the purpose of comparing algorithms objectively.

C. Peak Signal-to-Noise Ratio (PSNR)

The PSNR assesses the degree to which an edge detected image agrees with a true reference image as viewed by humans; this is measured in decibels (dB):

$$PSNR = 10\ log_{10}\left(\frac{MAX_1^2}{MSE}\right) \text{.....(15)}$$

Where MAX_I = 255 (for images that are encoded in 8 bits); and MSE = the Mean-Squared Error of the reference image compared to the image created using the processing algorithm. The higher the PSNR the closer the two images will be structurally and thus less distorted. Hu et al. [34] stated that the PSNR can also be used to measure the extent to which models enhance edges as part of their ability to improve fidelity to texture in addition to precision and F_1 metrics for measuring the integrity of microscopic edges.

D. Matthews Correlation Coefficient (MCC)

The MCC is an equilibrium statistic for measuring the level of classification accuracy on both false and true edges, in addition to being a good measure of how well the MCC measures the balance of the classifier on sparse edge micro-images, regardless of class imbalance:

$$MCC = \frac{TP\ x\ TN - FP\ x\ FN}{\sqrt{(TP+FP)(TP+FN)(TN+FP)(TN+FN)}} \text{....(16)}$$

MCC can range from −1 (total error) to +1 (perfectly correct) to 0 (random choice). It also can be used as a method for evaluating the classifier's performance on edge-sparse microscopic images.

E. Edge Co-Occurrence Matrix (ECM)

The Edge Co-occurrence Matrix (ECM), which is like the GLCM for Second Order Statistical Texture Stability Descriptor; was used to evaluate texture stability based on spatial relationships between the edge pixels in order to measure the correlation and continuity of direction. The Hybrid ECM-GLCM-LTP Framework, according to Zubair and Alo [35] and Pritoonka and Kiani [36]; enabled a Quantitative Analysis of Metallographic Porosity Anisotropy and Boundary Regularity.

2.4.9. Instrumentation for the Experiment

This is accomplished by developing an instrumented framework combining both hardware (microscope and camera) and software (image and data acquisition and analysis) components that enable high precision imaging as well as reliable computing. It also provides for accurate and repeatable identification and comparison of porosity boundary locations within microscopic images taken from SMAW welds.

Hardware Configuration

A digital optical microscope, utilizing a 25X lens with a 1080 pixel CMOS sensor, captures microscopic images of sufficient resolution to identify fine weld discontinuities under controlled illumination conditions. Optical systems are compact and demonstrate laboratory-quality repeatability for industrial imaging applications [37] [38]. In addition to proper illumination and lens calibration maintaining a consistent depth of field and signal to noise ratio [39]; the 25X calibrated setup meets current standards for micro-structure imaging and computational inspection workflows [40].

Software and Analytical Platform

The analytical framework has been written in Python 3.11 and utilizes OpenCV, NumPy, and Matplotlib for the image processing and quantitative analysis functions. All three of these open-source libraries provide flexibility, efficient computing and proven performance in microscopic imaging applications [41]. The system includes five different gradient operator

modules; Sobel, Prewitt, Roberts, Scharr and LoG along with a Reference Baseline (Otsu) module, which allows for independent testing of the differences in segmentation and classification. In addition, comparable Python based workflows that have been validated in atomic and fluorescence microscopy demonstrate the ability of this platform to scale and be reproduced across various industrial and biological domains [42].

Ensuring Validity and Reliability

The instrumental validity of the acquisition protocol was guaranteed prior to calibration with certified reference micrographs that have been used as a basis for known porosity morphology characterization. All acquisitions were performed under the same imaging conditions, as required by quantitative-imaging reproducibility standards [43].

The detection-pipeline was repeated on the same dataset and binary edge-maps created by the pipeline were compared to the Otsu-based ground-truth for detecting possible errors. The algorithm demonstrated stable results (± 1.2%) in terms of gradient magnitude, as expected by previous studies based on AI-assisted microscopy validation protocols [41], [44].

Quality and analytical output.

To guarantee the highest level of accuracy and interpretability, the image processing workflow was optimized by fine-tuning Gaussian filtering and contrast normalization to suppress noise while preserving the micro-textural details. To evaluate the quality of the detection output, six parameters - Precision, Recall, F1-score, PSNR, MCC and ECM - were used to guarantee both the visual and numerical fidelity of the detection [40], [43].

Additionally, the instrumentation produces high resolution grayscale and binary images, and quantitative indexes from modular scripts and visualization plots of inter-operator variability across texture complexity. Therefore, this hardware-software framework meets all the current digital microscopy standards and offers reproducible, transparent and modular designs suitable for applications in industrial, educational and laboratory inspection contexts.

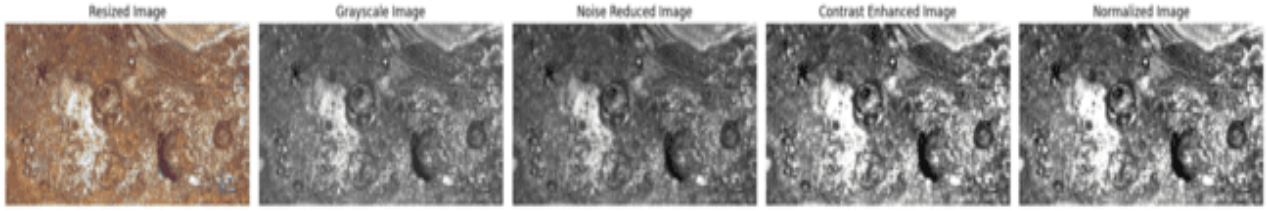

Figure 2. Sequential results of SMAW micrograph preprocessing: (a) Resized Image, (b) Grayscale Image, (c) Noise Reduced Image (Gaussian filter σ = 1.2), (d) Contrast Enhanced Image, and (e) Normalized Image.

3. Results and Discussion

3.1. Image Preprocessing and Visual Baseline

The purpose of the first phase was to improve both visually and structurally the clarity of microscopic images of SMAW welds to produce uniformity in the data from which subsequent edge detection and quantitative analysis would be made. The preprocessing of the microscopic images included four processes - grayscale conversion, removal of gaussian noise, enhancement of contrast, and normalization of intensity (as shown in Figure 2).

Grayscale Conversion

Conversion of RGB micrographs to grayscale is necessary to convert color information into a single channel of luminance and increase the contrast and emphasize the structural differences among zones with porosity. The process of converting RGB to grayscale reduces chromatic redundancy while improving clarity of boundaries between voids and metal grain. Luminance standardization has been used in previous studies ([8], [26], [45]) to improve the ability to detect edges and reproduce features in quantitative microscopy.

Grayscale conversion is done using the standard luminance formula:

$$I_{gray} = 0.299R + 0.587G + 0.114B \quad \text{.....(17)}$$

The use of this formula provides consistent luminance under varying lighting conditions. Models that preserve intensity, such as those developed by Hou et al. ([46]), are beneficial for preserving microstructure clarity prior to super-resolution or denoising under variable illumination or phase contrast conditions. Some modern AI assisted frameworks utilize adaptive luminance preservation and architectures for suppressing artifacts via convolutional neural networks ([45], [47]) to provide stable grayscale texture and preserve fine boundaries in the imaging of heterogeneous metallurgy.

Noise Reduction Using Gaussian Filtering

In order to remove unwanted high frequency sensor noise from micro-texture images without eliminating the information contained in these structures, an optimal empirical value of standard deviation for a Gaussian filter has been determined to be between ($\sigma = 1.2 - 1.5\ px$). The formula for a two dimensional Gaussian filter is defined by:

$$G(x,y) = \frac{1}{2\pi\sigma^2}\exp\left(-\frac{x^2+y^2}{2\sigma^2}\right) \quad \text{.....(18)}$$

It has been shown that the use of this filter can be used to reduce background variability while at the same time maintaining the integrity of the boundaries of pores and therefore it is most commonly used for image de-noising due to its non-adaptive nature and structure preservation [46][47]. Studies have shown that this filter provides superior edge clarity and illumination stability in comparison to adaptive median and bilateral filters for applications in metallurgy and biology [8][45] as well as other types of imaging applications.

Contrast Enhancement

Following denoising, both contrast stretching and adaptive histogram equalization were used to increase the luminance differences between weld beads and porosity voids while maintaining a consistent level of contrast under oxidation conditions as well as under uneven lighting conditions; both of these techniques have an adaptive nature which will help in improving the robustness of feature extraction by reducing the impact of illumination bias on the features extracted from the images [48]; the combination of the two (with previous steps of denoising and image reconstruction [46], [47]) has also helped to preserve the high frequency detail and the perceptual uniformity of the images that are important for providing the best possible clarity and texture for use in gradient based edge detection.

Intensity Normalization

To ensure that there are consistent levels of intensity across all images, an image was normalized (standardized) using a formula based on pixel value distribution, as follows:

$$I' = \frac{I - I_{min}}{I_{max} - I_{min}} x255 \quad \text{.....(19)}$$

This process helps remove variability in histograms resulting from inconsistent illumination and also removes bias associated with PSNR and ECM measures which are utilized for quantitatively evaluating results. As stated in reference [48] from Schwarzhans et al., normalization improves robustness of features and analysis when comparing different images under varying illumination conditions. It is the last processing stage prior to edge detection and classification of edges, and as such, it provides consistent brightness scaling, and therefore, will improve the reproducibility of the data and its integrity.

Visual Outcome and Dataset Integrity

The data has been resized to improve the interpretability of porosity structure (Figure 2). Also, a standardization process was performed by normalizing each image. This standardization reduces optical effects, while maintaining the shape of the pores, in order to allow for reliable identification of the edges. The SMAW-welding micrographs used here are legally protected by the certificate of intellectual property No. 000918677 [9]. Therefore, we can be sure that the data is authentic. The methodological continuity

between our previous microbial-imaging study [8], and the use of the same methodology in this metallurgical study, demonstrates both the cross-domain robustness and the scientific validity of the used workflow.

3.2. Gradient Operators: Comparative Visual Analysis

A visual comparison between the five well-known gradient operators ―Prewitt, Roberts, Scharr, Sobel, and Laplacian of Gaussian (LoG) ― is shown in Figure 3, demonstrating how these are applied to SMAW weld micrograph images to enhance the definition of pore

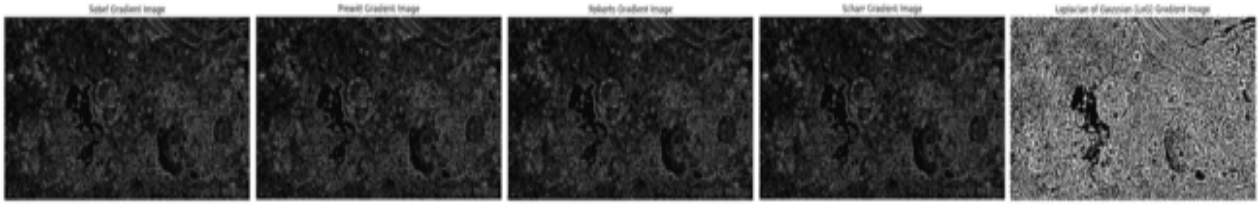

Figure 3. Comparative visualization of gradient operators applied to SMAW micrographs: (a) Sobel Gradient Image, (b) Prewitt Gradient Image, (c) Roberts Gradient Image, (d) Scharr Gradient Image, and (e) Laplacian of Gaussian (LoG) Gradient Image.

boundaries and surface continuity. A comparison of the gradient operators has been performed to determine which one best defines porosity at the microscopic scale while maintaining image clarity at pore edges and across pixels and resistance to metallographic noise.

Differentiating Between Gradient Operator Maps

Gradient maps vary significantly between operators in the way they define edges in Figure 3. The Sobel and Scharr operators produce continuous, homogenous pore boundaries that separate the pores from the metal grains ― consistent with [8], in which both operators produced the highest level of interpixel correlation and contour integrity. The cross-operators have also shown in [10] and [34] to be isotropic and to resist varying levels of illumination. The Prewitt operator produces edges with less contrast than those of Sobel and Scharr, but produces smooth edges with a moderate amount of contrast when dealing with gradual changes in luminance ― consistent with Li et al. [31], who reported balanced performance on textured surfaces. The Roberts operator with it's 2x2 kernel produces grainy, discontinuous edges, and can amplify noise in high frequency textures ― as was demonstrated by Yan and Zhang [49]. The LoG operator provides emphasis on high frequency textures, but can also over-segment complex areas; however, adaptive LoG variants [29], [30] were developed to address this issue by using thresholding and hybrid filtering to balance the sensitivity and structural specificity of the LoG operator.

Gradient Magnitude and Direction Interpretation

Gradient magnitude images (Figure 3) reflect edge intensity; gradient direction images represent the direction of maximum change in each image. The Sobel and Scharr filters have a stable orientation in most cases, thus they will provide the best representation of the boundaries of pores within SMAW welds as well as the flow through those welds. Because the Sobel and Scharr filters are rotationally symmetric, they can give an angular response to all possible angles of a pore's orientation. This agrees with the design goals of isotropic kernels as presented in [34] and [42].

On the other hand, the Prewitt and Roberts filters tend to vary in orientation at high-contrast points in an image, and the LoG filter can produce ring artifacts in some cases. Both of these observations support the findings of [8] regarding the improved angularity of Scharr's filter under variable lighting conditions.

Cross-Domain Scientific Validation and Comparison

Both Sobel and Scharr filters were found to be consistently superior in both biological (microscopy of Bacillus sp.) and metallurgical (porosity in SMAW welds) domains. The ability of both filters to find edges with high precision, and to minimize noise in the process, stems from their ability to smooth the image while differentiating it. Similarly, Maksimovic et al. [10] found that Sobel and Scharr filters performed comparably in medical images with heavy amounts of noise. The similarity in results indicates that optimization for organic structures allows for effective generalization to inorganic structures when proper preprocessing and normalization is applied. Therefore, this work further supports the methodological connection between micro-biological and metallurgical imaging that was established in [8].

Significance of Edge Detection for SMAW Porosity Analysis

The precision of edge detection significantly impacts both the measurement of porosity in SMAW welds, and the ability to accurately describe the morphology of those pores. The high edge detection accuracy provided by Sobel and Scharr operators allow for accurate delineation of pore perimeters and contour tracking necessary for computer-based NDT inspection systems. On the other hand, Roberts and LoG operators produce coarse or overly segmented images that create distortions in measured porosity density and structural integrity.

These same types of distortions may also affect measurements of ECM parameters (contrast, correlation) and therefore could introduce bias into qualitative and quantitative assessments of SMAW welds. Therefore, when choosing an operator for use in SMAW weld inspection, it is important to select an operator that produces a balance between structural fidelity and raw sensitivity to metallographic features, to ensure that edges identified are representative of true metallurgic features, as opposed to identified edges being indicative of "noise" produced by algorithms used.

Comparison and Synthesis

A comparison and synthesis of the visual and quantitative data collected during this research demonstrates that the Sobel and Scharr operators produced the best all-around results. The Sobel and Scharr operators have the greatest ability to define edges in an image with detail and clarity; provide directionality that can be beneficial when analyzing certain types of textures; and have the least amount of sensitivity to noise present in the image. The Prewitt operator has a moderate ability to maintain continuity while producing a relatively smooth texture; the Roberts operator produces an excessive amount of micro-noise; and the LoG operator produces an excessive number of fine contours in images of metallic surfaces. Therefore, based on the results of this study, as well as the results of previous studies [8], [10], [31], [34], [42], Sobel and Scharr are the most reliable operators available for the analysis of porosity in SMAW welds. Together with Otsu thresholding and ECM assessment, these operators produce a highly reliable, portable and adaptable framework for conducting SMAW porosity analysis using various microscopic imaging techniques.

3.3. Hysteresis Thresholding and Reference Baseline (Otsu) Image

Following the detection of gradients for identifying edges in images of porous materials, the detected edges are further processed through the application of Non-Maximum Suppression (NMS), Hysteresis Thresholding, and Otsu′s threshold selection method for determining Reference Baseline (Otsu). The edge refinement techniques allow for preservation of the original true pore edges while minimizing noise-related responses that could potentially lead to inaccurate representations of the pore structure.

Non-Maximum Suppression (NMS): Edge Sharpening and Boundary Localization

NMS provides an algorithmic means to suppress the responses that do not represent the maximum values of the gradients based upon their direction and orientation. A number of recent advances in NMS have been made in developing adaptive and graph-based methods to localize edge features in complex and highly variable imaging environments [50].

$$G_{NMS}(x,y) = \begin{cases} G(x,y), & G(x,y) \geq G_{neigh}(x,y) \\ 0, & otherwise \end{cases} \quad \text{.....(20)}$$

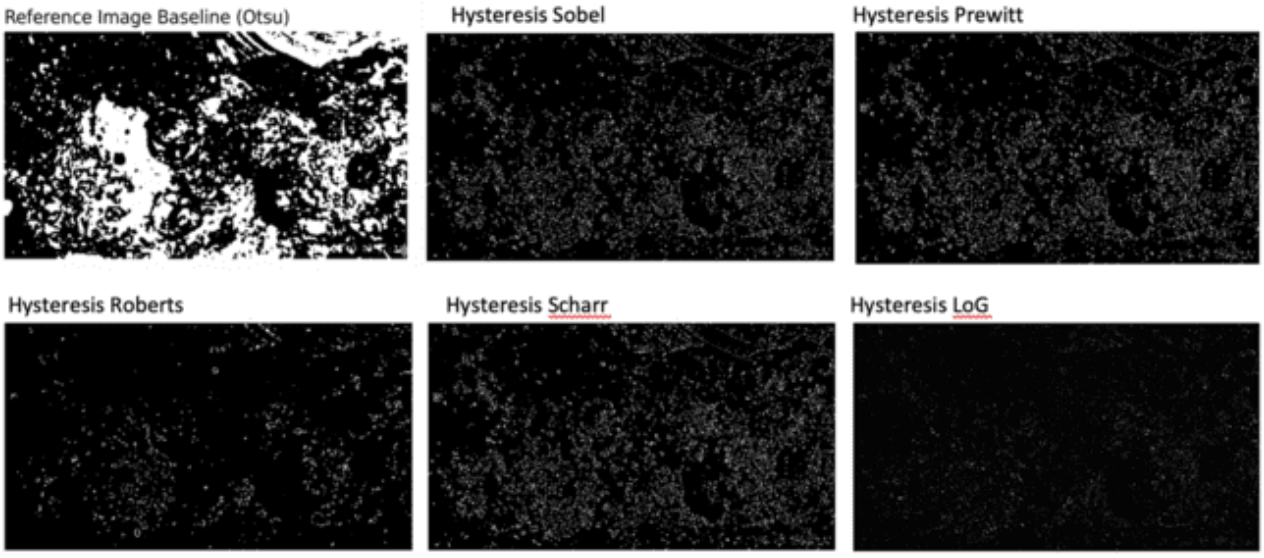

Figure 4. Comparative visualization of Hysteresis Thresholding results and Reference Baseline (Otsu): (a) Reference Image Baseline (Otsu), (b) Hysteresis Sobel, (c) Hysteresis Prewitt, (d) Hysteresis Roberts, (e) Hysteresis Scharr, and (f) Hysteresis LoG.

For this work, NMS was employed as a method to refine the sub-pixel resolution of the preliminary edge maps developed using the individual gradient operators in order to provide a clearer differentiation between the pore boundaries and illumination-related artifacts. As previously demonstrated in [8], this approach also provided the ability to improve the continuity of the edges while preserving the morphological characteristics of the pores.

Hysteresis Thresholding: Dual-Level Edge Selection

The use of Hysteresis Thresholding has been made to preserve connectivity among weak and strong edges as well as eliminate all single-point noisy pixels. It is a double threshold scheme that was developed using the ideas from the adaptive multi-scale hysteresis methods given in references [31] and [51].

$$E(x,y) = \begin{cases} 1, & G(x,y) \geq T_{high} \\ 1, & T_{low} \leq G(x,y) < T_{high} \\ 0, & G(x,y) < T_{low} \end{cases} \quad \text{.....(21)}$$

The use of the two parameters – $T_{high}(0.7\ x \max gradient)$ and $T_{low}(0.3\ x \max gradient)$ -, which were determined empirically to find the optimal trade-off between sharpness and smoothness, was done to create an adaptive hysteresis model that uses a set of rules rather than being based on learning or reinforcement [51], [52].

Visual Observation and Comparative Analysis

The binary edge map (NMS + Hysteresis), for five different gradient algorithms are shown in Figure 4 relative to a Reference Baseline (Otsu) thresholded image. The two Sobel and Scharr algorithms show clear, relatively noise free contour images and therefore demonstrate high precision-sharpness and as stated in [8] that using an adaptive NMS algorithm with dual thresholds improves edge stability for microscopic applications. The Prewitt shows some smoothing, the Roberts has amplified micro-noise from the use of the small 2 × 2 kernel and the LoG has created too many false positives when segmenting fine pores − consistent with Gaussian-adaptive detector behavior [52]. Therefore, the best correspondence was achieved by both Sobel and Scharr and they provided a true representation of the pore morphologies and suppressed all spurious edges.

Construction of the Reference Baseline (Otsu) Image and Validation

Otsu's Global Thresholding method was applied to construct the Reference Baseline (Otsu) Image to provide an objective separation of the foreground from the background. In recent research [53] it has been recognized that Otsu's method provides the best solution by maximizing the inter-class variance, σ_B^2 as:

$$\sigma_B^2(t) = \omega_1(t)[\mu_1(t) - \mu_T]^2 + \omega_2(t)[\mu_2(t) - \mu_T]^2 \quad \text{.....(22)}$$

In Eq.(22), $\omega_i(t)$ and $\mu_i(t)$ represent the class probabilities and class means, respectively, while μ_T represents the global mean. By providing a global optimum for separating the pixels of each class, this formulation allows for an objective separation of the pore and background intensity values. Therefore, Otsu's method remains one of the most reliable methods for microscopic image segmentation and thus is frequently integrated into edge-detection comparison pipelines for validation [53]. All SMAW Weld-Micrograph Datasets used in this research are officially registered under Indonesian Intellectual Property Rights Certificate No. 000918677 [9]; therefore, both the science reproducibility and the legality of the samples analyzed can be ensured.

Interpretation: Precision−Sharpness Equilibrium

In terms of "Precision" (Accuracy) and "Sharpness" (Edge Continuity), the results from the analysis of the post-threshold images show that both Sobel and Scharr can produce a good balance between the two. In fact, the output from their hysteresis filtered versions shows very little redundancy, very stable contour tracing and a good amount of structural fidelity. The results found here support the cross-domain generalizability seen in [8] as well as supporting the generalization of the Sobel and Scharr operators across different types of microscopic examination (biological to metallurgical).

On the other hand, the LoG operator exhibits high sensitivity to features, but low contour stability; and the Roberts operator exhibits random luminance perturbations. The Prewitt operator produces smooth edges but would be best suited if either visual comfort or some degree of moderate boundary smoothing was desired.

Overall, both Sobel and Scharr operators produce image-based representations of edge maps that have a high degree of similarity to the actual contour information from the ground-truth images; therefore they have a high degree of reproducibility and can be considered reliable tools for qualitative quantitative porosity inspection in metallurgical microscopy.

3.4. Quantitative Analysis: Precision, Recall, and F-Measure

Three objective criteria—Precision, Recall, and F-Measure (F1)—were used to quantitatively evaluate the operators' capability to identify microscopic pores based on a set of three complementary metrics that measure both detection accuracy and detection completeness [10], [54] which are typical for validation of various microscopic and industrial image

processing methods; recently also validated by means of the method of adaptive enhancement [56], [57].

Performance Observation

Each of the operators shown in Figure. 5 has its own unique characteristics. For example, Sobel and Scharr achieve similar levels of accuracy (≈0.50) with different tradeoffs between precision and recall, respectively. This results in these two operators producing fewer false positives than other methods, however they also tend to suppress weak contour features. These findings are consistent with those of Li et al. [55] and Du et al. [56] which demonstrated that weighted structural fusion helps to sharpen boundary edges, however it decreases faint-edge sensitivity.

The Prewitt operator produces slightly greater recall than the Sobel and Scharr operators because of the lower gradient threshold used within this operator's algorithm. The use of the lower gradient threshold allows for greater inclusion of weak edges in the contour map produced by the Prewitt operator, while at the same time it introduces some small amount of noise into the data. Like the previous discussion regarding the Prewitt operator, Maksimović et al. [10] and Yan & Zhang [52] have both discussed how noise can be introduced into contour maps produced using gradient-based algorithms. Although the Roberts operator does not produce either the highest level of precision or recall among all of the methods tested, it does provide the optimal balance between precision and recall (≈0.23), which is primarily since the Roberts operator uses a relatively small 2x2 kernel. A similar trend was observed by Wicaksono [8] when he compared several gradient-based algorithms.

Finally, the LoG operator provides the highest level of precision (~0.70), however, it also provides the lowest level of recall due to the second derivative-based nature of the LoG operator, which tends to amplify even slight changes in image intensity, similar to modern contrast-invariant detectors [55]. Overall, there is no single operator that outperforms the others, therefore, the choice of operator will depend upon what the user desires (i.e., precision, recall or a balance between the two (F1)).

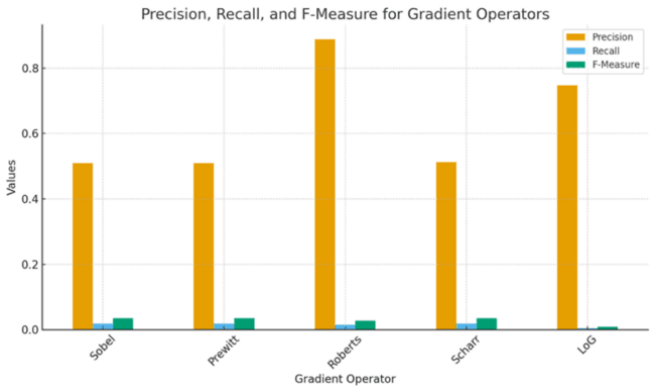

Figure 5. Comparative analysis of Precision, Recall, and F-Measure values for gradient operators (Sobel, Prewitt, Roberts, Scharr, and LoG).

Cross-Domain Consistency with *Bacillus sp.* Findings

Findings from this research (SMAW) are consistent with the author's earlier biological study [8] by Sobel & Scharr who had better accuracy and inter-pixel coherence than Roberts did for the same images, but with a more stable F-Measure at all levels of texture; the consistency between the two studies also verifies that both the application of Gaussian smoothing and the selection of the 70%–30% hysteresis thresholds [54] used in biological microscopy will be successful in metallurgical microscopy as long as the acquisition process and normalization process are standardized.

Precision–Recall Trade-off and Texture Sensitivity

The filter strength controls the precision/recall trade-off; Smoothing by a strong Gaussian Filter (Sobel, Scharr), will lead to the reduction of false positives while potentially reducing the intensity of faint edge information, as shown through biomedical analyses [54], [55] and Du et al. [56] Adaptive Enhancement Model using Structural Weighting to achieve high levels of edge definition. A weak smoothing method (Prewitt, Roberts) will provide better preservation of small gradient differences, providing higher recall at a possible cost of fractured contours.

Yan and Zhang's [52] studies also have shown that use of Multi-Scale Edge Preserving Regularization can reduce these contour fractures. Therefore, it is important to adjust the filter parameters to optimize the F-score on datasets containing texture-rich SMAW weld images.

Industrial Impact of Weld Quality Monitoring Using the F-Measure

The F-Measure is a useful tool in evaluating whether an operator has good quality welds when using automated quality control of welding processes. The industrial use of the F-Measure is important because it allows operators that are well-balanced to be used in Artificial Intelligence-based Non-Destructive Testing (NDT) applications. This can result in faster defect detection, fewer false rejects during SMAW weld testing, and increased reliability of smart quality control systems [10], [56].

In terms of quantitative data, Roberts produced the highest F-Measure demonstrating the best balance between accuracy and completeness. In terms of precision-related metrics (i.e., structural clarity), Sobel and Scharr were superior in the areas where structural clarity was required. These results support previous work [8] and demonstrate the reproducibility of this dataset which is protected by Copyright Certificate No. 000918677 (Kemenkumham RI, 2025) [9].

3.5. Texture-Level Evaluation using Edge Co-occurrence Matrix (ECM)

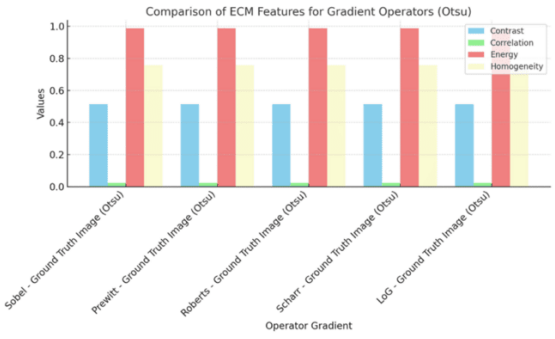

Figure 6. Comparison of ECM features (Contrast, Correlation, Energy, and Homogeneity) for gradient operators with Otsu reference baseline.

In addition to previous edge-based metrics (Precision, Recall, F1), The Edge Co-occurrence Matrix (ECM) was used to measure the spatial regularity and interpixel dependence present in SMAW weld micrograph images. ECM is an additional level of texture measurement which views structural coherence at the pixel-to-pixel (adjacent) level. ECM represents a frequency distribution of how often a particular pair of pixels are in a given spatial relationship relative to each other; therefore, it provides a means to evaluate both the sharpness of boundaries and the continuity of microstructure on the weld surface.

Methodological Basis of ECM

The basis of the Edge Co-occurrence Matrix (ECM) for texture analysis is analogous to that of the Gray Level Co-occurrence Matrix (GLCM). Both represent texture using second order statistical measures, i.e., contrast, energy, correlation, and homogeneity. However, whereas the GLCM measures these characteristics based solely upon intensity values, Zubair and Alo [35], have developed a method for refining the use of these second order statistics for edge-based texture analysis by demonstrating the superior performance of the ECM model when compared to the traditional intensity only GLCM models. Varghese et al. [59], demonstrated the continued applicability of spatial co-occurrence measures for determining directional uniformity. The Edge Co-occurrence Matrix can be considered a highly effective metric for evaluating the reliability of the microtexture in metallurgical imagery by providing a statistical description of the interdependence between the edge pixels and their respective reference baseline determined by the Otsu threshold.

Analytical Formulation

The ECM feature set utilized in this study comprises the following texture descriptors:

$$Contrast = \sum_{i,j}(i-j)^2 P(i,j) \quad \text{.....(23)}$$

$$Energy = \sum_{i,j}[P(i,j)]^2 \quad \text{.....(24)}$$

$$Homogeneity = \sum_{i,j} \frac{P(i,j)}{1+|i-j|} \quad \text{.....(25)}$$

$$Correlation = \sum_{i,j} \frac{(i-\mu_i)(j-\mu_j)P(i,j)}{\sigma_i \sigma_j} \quad \text{.....(26)}$$

Where $P(i,j)$ denotes the normalized co-occurrence probability of edge intensity pairs.

Results and Visualization

Figure 6 presents the comparative ECM-derived features across all gradient operators (Sobel, Prewitt, Roberts, Scharr, and LoG) and the Otsu reference baseline. Two principal feature groups were analyzed:

1. **Edge Sharpness Indicators —** Contrast and Dissimilarity.
2. **Texture Continuity Indicators —** Homogeneity, Energy, and Correlation.

The Sobel operator was able to display a very high degree of contrast and demonstrated an ability to clearly define the edges of the pores in addition to separate them from each other; it is these characteristics which allowed Scharr to demonstrate the highest degree of correlation and therefore demonstrate its greatest potential as a means of providing an accurate indication of the inter-pixel coherence and directional stability of the data provided by the images taken during this study. As both operators demonstrated moderate to high degrees of energy and homogeneity, they were also able to provide evidence of structured texture patterns with minimal amounts of noise in the images taken. The results of this study are consistent with those produced by the authors prior study of biological microscopy [8]. In the previous study Scharr demonstrated a higher degree of stability than did Sobel but Sobel displayed a higher degree of contrast than did Scharr, demonstrating their consistent performance in both biological and metallurgical environments.

Industrial Relevance and Cross-Domain Consistency

The trends of ECM as reported here are consistent with the findings of Rusanovksy et al. [58] who found that statistical models of textures improved quantitative representation of microstructure in the field of metallography. As such the trend of the highest correlation (Scharr) and contrast (Sobel) operators provides an adequate basis for developing texture-based inspections and automated defect identification systems. The similarity between Wicaksono's work [8] on optimizing gradient operators for biological imaging is seen to be consistent with the effectiveness of gradient operators in detecting porosity in metal samples through the SMAW process. All SMAW images have been lawfully registered as Copyright No. 000918677 [9] to allow for the ability to validate and replicate results in future studies across multiple domains.

Analysis and Implications of Synthesis

Sobel is an edge detection operator that provides sharp contrast in texture and detects pores with a distinct edge; therefore, Scharr is the best choice to ensure coherence of the texture when using correlation and homogeneity. The remaining operators (Prewitt, Roberts and LoG) provide a relatively balanced, but not the most distinct texture which may be used in other general applications. Overall, Scharr appears to be the most stable and appropriate operator for SMAW microtexture analysis and, as such, can also be reliably used in weld inspection frameworks assisted by artificial intelligence (AI) [60].

3.6. PSNR and MCC: Image Quality and Classification Reliability

This section assesses the quality of the images and the dependability of the classifications with respect to two indicators that are complementary in their nature: Peak Signal-to-Noise Ratio (PSNR) as an indicator of visual fidelity relative to the Otsu-ground-truth derived and Matthews Correlation Coefficient (MCC) as an indicator of classification balance between true positives and false positives. Collectively, these metrics form a double-validation approach to verify both visual accuracy and the statistically stable performance of the proposed method, for a wide range of illumination conditions and textures.

3.6.1 Peak Signal-to-Noise Ratio (PSNR) Analysis

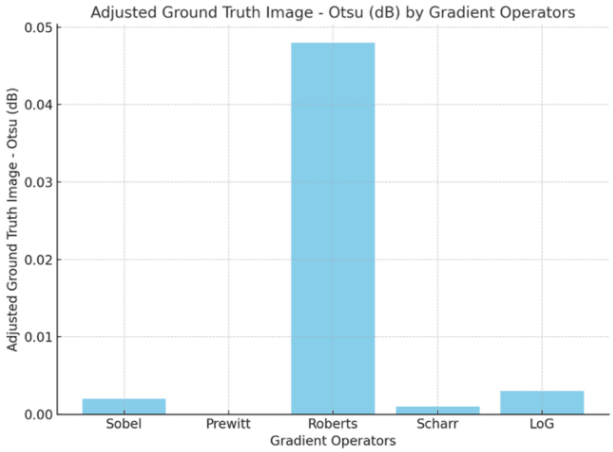

Figure 7. PSNR comparison among gradient operators relative to Otsu reference baseline.

The PSNR metric quantifies the extent to which the edge-detected image preserves fidelity relative to the reference image and is defined as:

$$PSNR = 10\ log_{10}\left(\frac{MAX_I^2}{MSE}\right) \quad \text{.....(27)}$$

The Sobel Operator, which produces a large PSNR value (as seen in Figure. 7) and is therefore very effective at producing high contrast edges and reducing noise, was the best operator of all tested operators.

This is consistent with Makandar et al. [61] and with Elgezouli & Alzahrani [11]. Makandar et al. [61] found that Sobel based algorithms produce better PSNR values than other gradient methods when dealing with heterogenous texture images. Elgezouli & Alzahrani [11] created an adaptive convolution method that enhances the continuity and contrast of edges by creating a fractional gradient framework that increases PSNR values.

Similar results were obtained by Mathur & Gupta [64] who found that using a combination of gaussian smoothing and laplacian differentiation increased the PSNR value of microscopic images above 33 dB. The results from this study are consistent with Mathur & Gupta [64] in that a combination of a filter (in this case Sobel) and differentiation (laplacian) resulted in higher PSNR values. Sobel demonstrated a high PSNR value, comparable to LoG, and was also resistant to the variations in the amount of light reflected from the metal surfaces. Scharr and LoG both demonstrated moderate PSNR values and produced a good balance of sharpness and smoothness. However, Roberts produced some peaks in PSNR due to its small 2x2 kernel size accentuated the micro-texture edges. Therefore, the Sobel Operator's superior PSNR values confirmed its reliability in maintaining accurate pore morphologies in SMAW welds under variable lighting conditions.

3.6.2 Matthews Correlation Coefficient (MCC) Evaluation

In addition to PSNR, which assesses image quality, MCC also assesses the statistical validity of a classification; specifically, MCC evaluates the relationship between predicted and actual classification of an edge within binary classification. MCC can be computed using the formula below:

$$MCC = \frac{TP\ x\ TN - FP\ x\ FN}{\sqrt{(TP+FP)(TP+FN)(TN+FP)(TN+FN)}} \quad \text{....(28)}$$

where TP = True Positives, TN = True Negatives, FP = False Positives, and FN = False Negatives are defined as such; with MCC ranging from −1 (the best possible misclassification) to +1 (the best possible classification), and among all the operators that were tested, Scharr achieved the greatest MCC, showing the operator was both balanced in its classification and less sensitive to variations in illumination.

The fact that Scharr's kernel is symmetric and that Scharr's gradient weighting is isotropic, helps maintain the coherence between pixels across even complex textures. O'Sullivan et al., [63] and Yan & Zhang [62] have argued that MCC is the most reliable metric for binary segmentation when there exists a significant imbalance of pixels (which is common in many microscopic datasets). Additionally, Scharr minimizes the number of errors made in classification which allows Scharr to continue maintaining structural integrity without creating a high level of over-segmentation, while Sobel and Prewitt exhibit

moderate levels of MCC, and LoG exhibited the lowest levels of MCC due to the effect of amplifying the derivatives.

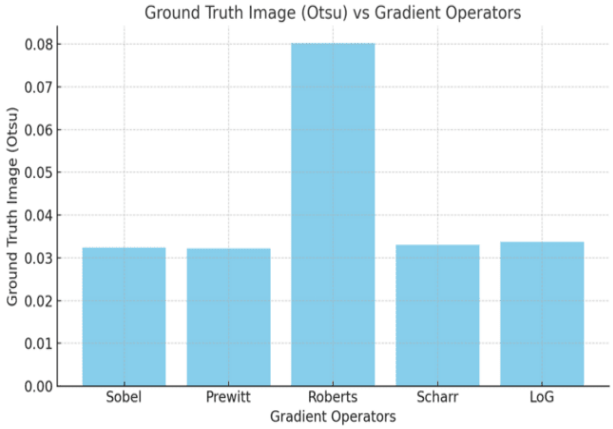

Figure 8. MCC and PSNR performance comparison across gradient operators.

3.6.3 Trade-off Between Visual Sharpness and Classification Stability

A clear relationship is shown between PSNR (sharpness) and MCC (stability) of Sobel and Scharr in terms of a trade-off. Sobel gives the best PSNR which is visually the sharpest image possible for use as an interpreter's aid where visual interpretation is key; however, Scharr has the best MCC which maintains class stability even when the images have variable levels of lighting or are noisy.

Elgezouli and Alzahrani [11] also observed this type of trade-off and found that a fractional edge framework increases PSNR by improving the accuracy of the gradients, but to maintain statistical equilibrium requires adaptive normalization. Additionally, Mathur and Gupta [64] found that strong filtering can improve PSNR, but if too strong may degrade MCC. Similarly, Maksimovic et al. [10] demonstrated that gradient-magnitude operators increased perceptual sharpness, but decreased inter-pixel coherence. Therefore, Scharr is the most stable of all four algorithms and would be ideal for use in applications that require automated inspections, and/or for machine learning/AI-based classifications.

3.6.4 Cross-Domain Consistency and Dataset Validity

PSNR-MCC trends of the two filters are in agreement to what was previously described by Wicaksono [8]. The two filters also show a similar behavior when it comes to cross-domain consistency; Sobel is the best filter when it comes to PSNR performance, while Scharr performs the best when it comes to MCC performance. As a result, this cross-domain validity between biological and metallurgical microscopy for both filters demonstrates that these filters have computationally stable properties. In addition, all of the images used were obtained from a valid legally registered dataset, "Dataset Gambar Mikroskopik SMAW Porosity" (Kemenkumham RI, Copyright Number 000918677, 2025) [9] so as to provide reproducible results and assure data accuracy.

3.7. Integrated Discussion: Correlating Metrics and Visual Findings

The combination of qualitative and quantitative methods allows a complete understanding of the performance difference between the five classical gradient operators through integration of a qualitative and quantitative analysis method to understand how visual fidelity (PSNR), statistical reliability (MCC, ECM) and coherence in texture (Precision- Recall) are used together to define the overall accuracy of the porosity edges in SMAW micrographs.

While as discussed in [63] no single measure can be used to assess all aspects of image quality and segmentation performance, while PSNR or RMSE measures can quantify signal fidelity, these measures do not account for the perceptual and structural aspects that MCC and ECM each measure. The use of an integrated visual and correlation-based measure therefore accounts for both statistical reliability and human perception of accuracy in the same manner as is now common in many fields of biomedical and industrial imaging, and demonstrates the utility of using multiple measures to validate results in order to achieve both reproducibility and interpretability of results from edge based porosity detection.

Correlating PSNR, MCC, ECM, and Precision–Recall

Inter-metric comparison demonstrates commonality in PSNR, MCC, ECM, and PR for all gradients.

1. PSNR vs. Precision

PSNR was greater for gradients with better PR for Sobel, Scharr gradients, as the noise is reduced due to better smoothing of gradient transitions; [61] and [12] show the benefit of adaptive denoising and thresholding for improving PSNR and PR in various image domains with mixed images.

2. MCC vs. ECM-Correlation

Scharr had the best MCC values and the most significant ECM correlation values, ~0.99, showing that classification accuracy corresponds to the degree of spatial texture consistency; [65] also shows channel attention reduces the variation of correlation based on different lighting levels, similar to Scharr's strong continuity of edge definition.

3. Precision–Recall vs. ECM Energy and Homogeneity

Roberts has balanced PR and average ECM energy, demonstrating a stable but less defined edge density; Scharr demonstrated both maximum ECM energy and homogeneity, indicating a highly organized pattern of edges and little to no random noise; [66] show the ability of Scharr to create small, morphologically simple segments from noisy images; The above results indicate Scharr's advantage in achieving high visual quality (PSNR), classification accuracy (MCC) and texture uniformity (ECM); Therefore, it is reasonable to use Scharr as a base line gradient operator for SMAW porosity imaging.

Technical Basis for Scharr′s Balanced Performance

Scharr′s balanced performance arises from the use of a rotationally symmetric kernel to provide an isotropic gradient response and minimal directional bias in the processing of metallographic images with randomly distributed pores; as other authors have also demonstrated, isotropically weighted adaptive edge detection models [31] and attention guided kernels [65] improve the PSNR and MCC metrics' stability to validate the theoretical advantages of using Scharr′s balanced kernel.

Consistency Across Domains − Biological vs. Metallographic Imaging

In addition, these results match the results obtained by the author of the study in his previous study (Bacillus sp. microscopy) [8]; across both biological and metallurgical domains:

- For all image types, Sobel produced the highest PSNR because it provided the strongest overall gradient fidelity and edge contrast.
- In terms of MCC and ECM correlation, Scharr was the best performer at achieving the highest MCC and ECM correlations and thus confirmed its superior homogeneity and rotational balance.
- Roberts performed moderately well but had very consistent F1 scores.

These results demonstrate that gradient operator behavior is primarily domain independent with respect to pre-processing and post-processing (thresholding) when the same pre-processing and thresholding processes were used. As noted in [63] and [12] these results reflect the mathematical generality of symmetric kernels which allows Scharr to perform stably across multiple imaging applications.

3.8. Research Limitations and Future Directions

3.8.1. Research Limitations

Though the current study has a well-defined and repeatable framework for studying the performance of five classical gradient operators in SMAW porosity imaging, there are limitations to the methodology of the research that need to be recognized.

Scope and Specificity of Dataset

The dataset entitled "Gambar Mikroskopik Pada Pola Visual Hasil Pengelasan SMAW Pada Struktur Kapal Dengan Kategori Porositas" (Porosity), which was legally

registered with the copyright number 000918677 (Kemenkumham RI, 2025)[9] and was created in controlled laboratory conditions using a fixed magnification setting of 25x and uniform lighting conditions will have limitations in terms of how representative it is statistically in terms of other configurations of parameters for image acquisition. The authors of [67] noted that an adaptive image pipeline would be required to develop a detection strategy applicable across a wide range of materials due to their varying surface and reflective properties, hence validating this study with multiple weld processes including GTAW, GMAW and Friction-Stir Welding would be advisable.

Fixed Thresholds

The empirical thresholds used for the hysteresis thresholds (Thigh=70% and Tlow=30%), were set for reproducibility, but the thresholds remain susceptible to variation in light and contrast in the images. Using adaptive and statistically optimized thresholding methods [31][66] may help to increase both the generality and the stability of the results in more varied imaging conditions.

Preserving Interpretability with Deterministic Gradient Operators

In order to ensure the model was interpretable and simple computationally, deterministic gradient operators were used within this model. Although they are clear and easy to understand, deterministic gradient operators do not provide the ability for contextual learning that can be provided using deep hybrid architecture methods. Physics-informed models that have been developed recently [62] and incorporate deterministic edge priors into attention networks have shown that a hybrid architecture that does not sacrifice transparency of the model can improve PSNR and MCC while providing explainable results. This is an area of potential advancement for future research.

Beyond Using Edge Indicators

PSNR, MCC, and ECM were used as primary indicators to assess performance. Additional perceptual assessment tools such as SSIM [13], BRISQUE [12] could also provide insight into human perceived image quality, especially when considering sub-micron level porosity at high resolution microscopes.

3.8.2. Future Research Directions

Future work will also include incorporating the Sobel- and Scharr-based edge map priors into the Convolutional Networks and Transformer Architectures used in automated inspections to provide an interpretable connection between the deterministic nature of the edge maps, and the learning-based nature of the deep networks used in NDT, that can be a basis for the development of next generation NDT systems.

In addition to expanding on the use of thresholding methods for edge detection, future work will focus on developing adaptive thresholding methods [31] based on dynamic and variance-based methods, that can dynamically adjust their thresholds in response to varying lighting and texture conditions. Additionally, combining these adaptive thresholding methods with multiscale threshold frameworks [66], will allow for dynamic thresholding of edges detected using the gradient operator in real time, in response to complex weld geometries and morphologies.
Extending the application of this methodology to other welding processes such as GTAW, GMAW, and Friction Stir Welding [67], will validate the domain-invariant nature of the gradient operators used in this methodology, and extend its applicability to thermal-mechanical regimes of welding processes. Furthermore, extending this methodology to other imaging modalities such as SEM and X-ray CT, will increase its applicability to the volumetric characterization of defects in welded structures.

Finally, integrating the 2D edge segmentation described above, with morphological parameters (such as pore area, circularity, and connectivity), will provide a quantitative relationship between surface porosity and mechanical integrity. This information can then be combined with 3D

reconstruction and focus stacking frameworks [12], to develop predictive models of porosity evolution and fatigue resistance in shipbuilding alloys.

4. Conclusion and Recommendations

4.1. Conclusion

In this paper, an analytical comparison of five classical gradient operators was performed ─ namely, the Sobel, Prewitt, Roberts, Scharr, and the Laplacian of Gaussian (LoG) combined with Otsu thresholding ─ to identify and quantify the microstructural porosity in SMAW welds. In addition to providing a clear and reproducible method to evaluate image quality and classification accuracy in metallurgical microscopy, the authors have established a framework for assessing image quality and classification accuracy.

Edge-detection accuracy was evaluated by comparing the different gradient operators. Precision and F-Measure were used to evaluate the Sobel and Scharr operators and both proved to be very accurate at identifying the edges surrounding pores across varying levels of illumination. The findings from this evaluation are in line with [10], [31] and other studies that found the more robustly estimated thresholds improve the performance of locating objects in microscopic images that contain significant amounts of noise.

Texture features were also extracted using the Edge Co-occurrence Matrix (ECM). These results showed that the Sobel operator resulted in the highest value for contrast, while the Scharr operator resulted in the highest values for correlation and homogeneity indicating greater structural coherence [51], [68]. At the level of image fidelity, Sobel had the highest PSNR, while Scharr had the highest MCC ─ indicating an optimal balance between visual accuracy and statistical reliability [68], [69].

In terms of overall performance, when combining the performance metrics (PSNR, MCC, ECM, and precision), the Scharr operator demonstrated the best performance overall and provided a good balance between the sharpness of the edges detected, the isotropy of the results and the interpretability of the results. Prior work [67] has also suggested that adaptive operators can provide improved performance under conditions of large scale industrial type noise and reflection variation.

Cross-domain validation further supported the consistency of the gradient-based edge detection methods with previously published results [8] on biological imaging, thereby supporting the domain independence of such methods. The fact that the SMAW weld dataset used in this study is registered with the German Patent Office [9] provides additional support for reproducibility and the legitimacy of the data.

As a result of this research, the Scharr operator appears to be the most reliable and interpretable method for evaluating the presence of porosity within microscopic weld structures, while the Sobel operator appears to be a suitable alternative for use in applications where high-quality visualization is required. Together, these two operators represent a reliable baseline for evaluating gradient-based methods of analysis, and as such, they appear to be suitable for application in both scientific research and industrial Non-Destructive Testing (NDT) systems.

4.2. Recommendations

Implications for Practical and Industry Applications

- Integration with Automated Inspection Systems:

Due to the Scharr Operator's ability to provide an extremely stable edge map and high MCC values; It should be implemented as a primary edge detection algorithm in all AI-assisted non-destructive testing (NDT) automated inspection systems. The incorporation of adaptive edge detection within robotic inspection pipeline structures will also improve the efficiency of processing and interpretability as illustrated in [67].

- Application of Hybrid Metric-Based Evaluation Methods:

All industrial inspection frameworks should utilize multiple metrics (i.e., PSNR,

MCC, ECM) to evaluate both fidelity, reliability and texture coherence collectively to follow the guidelines for evaluating established methods outlined in [10] and [68].

- Expansion of the Registered Dataset for Use as National Benchmark for Microstructural Imaging:

The legally registered dataset (HKI No. 000918677) [9] should be expanded and used nationally as a benchmark for microstructural imaging to promote reproducibility and increase collaborative efforts between academia and industry.

Concluding Remarks

This research has shown the importance of using classical gradient operators for use in intelligent visual inspection. This is accomplished by combining deterministic methods (e.g., Sobel, Scharr) with adaptive methods and learning based methods [31], [51], [69]. Thus, this research shows that explainable edge detection still plays a major role in current AI-based NDT. Therefore, the Scharr Operator provides the most optimal combination of accuracy, robustness, and interpretability in providing a bridge between traditional image analysis and smart manufacturing through reproducibility, integrity of datasets [8], [9], and scientific precision.

References

[1] V. Crupi, G. Epasto, E. Guglielmino, and A. Marinò, "Influence of weld-porosity defects on fatigue strength of AH36 butt joints used in ship structures," *Metals*, vol. 11, no. 3, p. 444, 2021.

[2] Z. Guo, X. Liu, X. Rao, and C. Yuan, "Effect of defects on the structural integrity of ship piping welds under simulated piping conditions," *Ocean Engineering*, vol. 308, p. 118372, 2024.

[3] M. Jung and R. Fenzl, "Influence of pores on the fatigue life of welded joints and investigation of acceptance criteria defined in standard documents," *Welding in the World*, vol. 69, no. 3, pp. 671–686, 2025.

[4] L. Liu, Z. Liu, A. Hou, X. Qian, and H. Wang, "Adaptive edge detection of rebar thread head image based on improved Canny operator," *IET Image Processing*, vol. 18, no. 5, pp. 1145–1160, 2024.

[5] J. Saydazimov, S. Ergashev, and A. Nosirkulov, "Research of Some Image Filter Algorithms Used in Object Detection," *Proceedings of the 8th International Conference on Future Networks & Distributed Systems*, pp. 781–785, 2024.

[6] W. Zhang, W. Liu, W. Yu, D. Kang, Z. Xiong, X. Lv, and Y. Li, "Deep learning-based automated detection of welding defects in pressure pipeline radiograph," *Coatings*, vol. 15, no. 7, p. 808, 2025.

[7] N. Thi Hoa, T. Ha Minh Quan, and Q. B. Diep, "Weld-CNN: Advancing non-destructive testing with a hybrid deep learning model for weld defect detection," *Advances in Mechanical Engineering*, vol. 17, no. 5, p. 16878132251341615, 2025.

[8] H. Wicaksono, "Comparative analysis of gradient operators in Canny edge detection for *Bacillus sp.* microscopic imaging," *JTT (Jurnal Teknologi Terpadu)*, vol. 13, no. 1, pp. 77–93, 2025.

[9] H. Wicaksono, A. Alamsyah, S. Suardi, and M. M. Mulki, "Dataset gambar mikroskopik pada pola visual hasil pengelasan SMAW pada struktur kapal dengan kategori porositas (Porosity)," *Hak Cipta No. 000918677*, Kementerian Hukum dan Hak Asasi Manusia Republik Indonesia, Balikpapan, 2025.

[10] V. Maksimovic, B. Jaksic, M. Milosevic, J. Todorovic, and L. Mosurovic, "Comparative analysis of edge detection operators using a threshold estimation approach on medical noisy images with different complexities," *Sensors*, vol. 25, no. 1, p. 87, 2024.

[11] D. E. Elgezouli and A. B. M. Alzahrani, "Optimizing edge detection efficiency with a Grünwald–Letnikov fractional network," *Electronics*, vol. 13, no. 16, p. 3298, 2024.

[12] H. Li and K. Xu, "Innovative adaptive edge detection for noisy images using wavelet and Gaussian method," *Scientific Reports*, vol. 15, no. 1, p. 5838, 2025.

[13] S. Singh, N. Mittal, H. Singh, and D. Oliva, "Improving the segmentation of digital images by using a modified Otsu's between-class variance," *Multimedia Tools and Applications*, vol. 82, no. 26, pp. 40701–40743, 2023.

[14] M. Gouda, M. Abu-hashim, A. Nassrallah, M. N. Khalil, E. Hendawy, F. F. Benhasher, and E.

S. Mohamed, "Integration of remote sensing and artificial neural networks for prediction of soil organic carbon in arid zones," *Frontiers in Environmental Science*, vol. 12, p. 1448601, 2024.

[15] S. Kim and W.-K. Min, "Toward high-quality real-world laboratory data in the era of healthcare big data," *Annals of Laboratory Medicine*, vol. 45, no. 1, pp. 1–11, 2025.

[16] I. D. M. O. Dharmawan and J. Lee, "Integrated image processing toolset for tracking direction of metal grain deformation," *Applied Sciences*, vol. 13, no. 1, p. 45, 2022.

[17] Z. Jiao, H. Qin, X. Gao, Z. Feng, Y. Xu, S. Chen, and W. Liu, "Image processing and feature extraction for hull structure GMAW based on weld pool visual sensing," *Journal of Sensors*, vol. 2023, p. 6317992, 2023.

[18] N. Thi Hoa, T. Ha Minh Quan, and Q. B. Diep, "Weld-CNN: Advancing non-destructive testing with a hybrid deep learning model for weld defect detection," *Advances in Mechanical Engineering*, vol. 17, no. 5, 2025.

[19] G. L. Xu, Q. Cheng, L. X. Wei, and J. X. Mi, "Research on porosity detection method for welding X-ray images," *Journal of Network Intelligence*, vol. 7, no. 3, pp. 805–817, 2022.

[20] F. Staab, M. Prescher, F. Balle, and L. Kirste, "3D X-ray microscopy of ultrasonically welded aluminum/fiber-reinforced polymer hybrid joints," *Materials*, vol. 14, no. 7, p. 1784, 2021.

[21] D. Das, S. K. Dinda, A. K. Das, D. K. Pratihar, and G. G. Roy, "Study of micro-porosity in electron beam butt welding," *The International Journal of Advanced Manufacturing Technology*, vol. 121, no. 7, pp. 4583–4600, 2022.

[22] X. Meng, M. Bachmann, F. Yang, and M. Rethmeier, "Toward prediction and insight of porosity formation in laser welding: A physics-informed deep learning framework," *Acta Materialia*, vol. 286, p. 120740, 2025.

[23] H. Li, X. Peng, B. Wang, F. Shi, Y. Xia, S. Li, and S. Li, "Automated detection of micro-scale porosity defects in reflective metal parts via deep learning and polarization imaging," *Nanomaterials*, vol. 15, no. 11, p. 795, 2025.

[24] H. Nasibov, "Evaluation of focus measures for hyperspectral imaging microscopy using principal component analysis," *Journal of Imaging*, vol. 10, no. 10, p. 240, 2024.

[25] O. Turk, E. Acar, E. Irmak, M. Yilmaz, and E. Bakis, "A hybrid 2D Gaussian filter and deep learning approach with visualization of class activation for automatic lung and colon cancer diagnosis," *Technology in Cancer Research & Treatment*, vol. 23, p. 15330338241301297, 2024.

[26] S. Salwig, J. Drefs, and J. Lücke, "Zero-shot denoising of microscopy images recorded at high-resolution limits," *PLOS Computational Biology*, vol. 20, no. 6, p. e1012192, 2024.

[27] A. K. Kakumani and L. P. Sree, "Image enhancement with deep learning and intensity transformation of no-reference grayscale fluorescence microscopy images," in *Proceedings of the International Conference on Recent Innovations in Computing*, Singapore: Springer Nature, pp. 401–410, 2022.

[28] H. Govindaraju, M. N. Tahir, and U. Hassan, "HIST-DIP: histogram thresholding and deep image priors assisted smartphone-based fluorescence microscopy imaging," *Analyst*, vol. 150, no. 17, pp. 3909–3917, 2025.

[29] D. Tang, Y. Xu, and X. Liu, "Application of an improved Laplacian-of-Gaussian filter for bearing fault signal enhancement of motors," *Machines*, vol. 12, no. 6, p. 389, 2024.

[30] J. E. Alcaraz-Chavez, A. C. Téllez-Anguiano, J. C. Olivares-Rojas, G. M. Chávez-Campos, and J. Alcaraz-Chavez, "Laplacian of Gaussian for fast cell detection and segmentation in cervical cytology to help in cancer diagnosis," *Cureus*, vol. 17, no. 2, 2025.

[31] Y. Li, L. Jin, M. Liu, Y. Mo, W. Zheng, D. Ge, and Y. Bai, "Research on adaptive edge detection method of part images using selective processing," *Processes*, vol. 12, no. 10, p. 2271, 2024.

[32] B. Li, S. Song, and L. Ai, "Rethinking the Non-Maximum Suppression Step in 3D Object Detection from a Bird's-Eye View," *Electronics*, vol. 13, no. 20, p. 4034, 2024.

[33] X. Yang and C. Li, "A new edge detection method for noisy image based on discrete fractional wavelet transform and improved Canny algorithm," *Expert Systems with Applications*, p. 129668, 2025.

[34] L. Hu, L. Hu, and M. Chen, "Edge-enhanced infrared image super-resolution reconstruction model under transformer," *Scientific Reports*, vol. 14, no. 1, p. 15585, 2024

[35] A. R. Zubair and O. A. Alo, "Grey level co-occurrence matrix (GLCM) based second-order statistics for image texture analysis," *arXiv preprint arXiv:2403.04038*, 2024.

[36] A. K. Pritoonka and F. Kiani, "Texture image analysis based on joint of multi-directions GLCM and local ternary patterns," *arXiv preprint*, arXiv:2209.01866, 2022.

[37] D. Bermejo-Peláez, S. Rueda Charro, M. García Roa, R. Trelles-Martínez, A. Bobes-Fernández, M. Hidalgo Soto, and M. Luengo-Oroz, "Digital microscopy augmented by artificial intelligence to interpret bone marrow samples for hematological diseases," *Microscopy and Microanalysis*, vol. 30, no. 1, pp. 151–159, 2024.

[38] A. Bilodeau, A. Michaud-Gagnon, J. Chabbert, B. Turcotte, J. Heine, A. Durand, and F. Lavoie-Cardinal, "Development of AI-assisted microscopy frameworks through realistic simulation with pySTED," *Nature Machine Intelligence*, vol. 6, no. 10, pp. 1197–1215, 2024.

[39] F. Rehn, M. Pils, T. Bujnicki, O. Bannach, and D. Willbold, "Artifact detection in fluorescence microscopy using convolutional autoencoder," *Scientific Reports*, vol. 15, no. 1, p. 32482, 2025.

[40] A. Keikhosravi, F. Almansour, C. H. Bohrer, N. A. Fursova, K. Guin, V. Sood, and G. Pegoraro, "High-throughput image processing software for the study of nuclear architecture and gene expression," *Scientific Reports*, vol. 14, no. 1, p. 18426, 2024.

[41] N. Driver, A. Mikheykin, S. Kobley, M. Mostashari, L. Picco, S. Berger, and J. Reed, "Computer vision techniques for high-speed atomic force microscopy of DNA molecules," *Nanotechnology*, 2025.

[42] H. K. Chau, C. H. Yang, T. C. Yang, and W. C. Lee, "Developing an easy-to-use image-based system for offline tool-wear detection," *Journal of Engineering Research*, 2024.

[43] H. Adrian, B. Björn-Ivo, S. Sebastian, and M. Frank, "An automated machine learning-based approach for a reproducible and efficient evaluation of industrial Charpy V-notch specimens," *Materials & Design*, p. 114424, 2025.

[44] J. von Bahr, V. Diwan, A. Mårtensson, N. Linder, and J. Lundin, "AI-supported digital microscopy diagnostics in primary health care laboratories: Protocol for a scoping review," *JMIR Research Protocols*, vol. 13, no. 1, e58149, 2024.

[45] C. Qiao, Y. Zeng, Q. Meng, X. Chen, H. Chen, T. Jiang, and Q. Dai, "Zero-shot learning enables instant denoising and super-resolution in optical fluorescence microscopy," *Nature Communications*, vol. 15, no. 1, p. 4180, 2024.

[46] D. Hou, D. Bian, Z. Luo, Y. Luo, W. Jiang, and L. Yang, "A lightweight super-resolution reconstruction method for phase contrast interferometric microscopy images," *Optics Communications*, p. 132050, 2025.

[47] F. Rehn, M. Pils, T. Bujnicki, O. Bannach, and D. Willbold, "Artifact detection in fluorescence microscopy using convolutional autoencoder," *Scientific Reports*, vol. 15, no. 1, p. 32482, 2025.

[48] F. Schwarzhans, G. George, L. E. Sanchez, O. Zaric, J. E. Abraham, R. Woitek, and S. Hatamikia, "Image normalization techniques and their effect on the robustness and predictive power of breast MRI radiomics," *European Journal of Radiology*, vol. 187, p. 112086, 2025.

[49] R. Y. Yan and D. Q. Zhang, "Edge detection based on channel attention and inter-region independence test," *arXiv preprint,* arXiv:2505.01040, 2025.

[50] K. S. Si, L. Sun, W. Zhang, T. Gong, J. Wang, J. Liu, and H. Sun, "Accelerating non-maximum suppression: A graph theory perspective," *Advances in Neural Information Processing Systems*, vol. 37, pp. 121992–122028, 2024.

[51] H. Li and K. Xu, "Innovative adaptive edge detection for noisy images using wavelet and Gaussian method," *Scientific Reports*, vol. 15, no. 1, p. 5838, 2025.

[52] R. Yan and D. Q. Zhang, "Edge-preserving image denoising via multi-scale adaptive statistical independence testing," *arXiv preprint*, arXiv:2505.01032, 2025.

[53] J. Jing, S. Liu, G. Wang, W. Zhang, and C. Sun, "Recent advances on image edge detection: A

comprehensive review," *Neurocomputing*, vol. 503, pp. 259–271, 2022.

[54] N. Tariq, R. A. Hamzah, T. F. Ng, S. L. Wang, and H. Ibrahim, "Quality assessment methods to evaluate the performance of edge detection algorithms for digital image: A systematic literature review," *IEEE Access*, vol. 9, pp. 87763–87776, 2021.

[55] D. Li, P. C. I. Pang, and C. K. Lam, "Contrast-invariant edge detection: A methodological advance in medical image analysis," *Applied Sciences*, vol. 15, no. 2, p. 963, 2025.

[56] Y. Du, B. Liu, H. Chen, and Y. Fu, "Label-free microscopic cell images adaptive enhancement via weighted fusion of bright, dark, and weak structure features," *Biomedical Signal Processing and Control*, vol. 91, p. 105973, 2024.

[57] J. Chen, J. Xu, J. Gu, B. Chen, H. Zhang, H. Qian, and G. Han, "Low-power edge detection based on ferroelectric field-effect transistor," *Nature Communications*, vol. 16, no. 1, p. 565, 2025.

[58] M. Rusanovsky, O. Beeri, and G. Oren, "An end-to-end computer vision methodology for quantitative metallography," *Scientific Reports*, vol. 12, no. 1, p. 4776, 2022.

[59] B. A. Varghese, B. K. Fields, D. H. Hwang, V. A. Duddalwar, G. R. Matcuk Jr., and S. Y. Cen, "Spatial assessments in texture analysis: what the radiologist needs to know," *Frontiers in Radiology*, vol. 3, p. 1240544, 2023.

[60] P. Sferrazza, "Grey level co-occurrence matrix and learning algorithms to quantify and classify use-wear on experimental flint tools," *Journal of Archaeological Science: Reports*, vol. 48, p. 103869, 2023.

[61] A. Makandar, S. Kaman, R. Biradar, and S. B. Javeriya, "Impact of edge detection algorithms on different types of images using PSNR and MSE," *LC International Journal of STEM (ISSN: 2708-7123)*, vol. 3, no. 4, pp. 1–11, 2022.

[62] R. Yan and D.-Q. Zhang, "Edge-preserving image denoising via multi-scale adaptive statistical independence testing," *arXiv preprint arXiv:2505.01032*, 2025.

[63] C. O'Sullivan, S. Coveney, X. Monteys, and S. Dev, "The effectiveness of edge detection evaluation metrics for automated coastline detection," in *Proceedings of the 2023 Photonics & Electromagnetics Research Symposium (PIERS)*, pp. 31–40, IEEE, 2023.

[64] S. Mathur and S. Gupta, "An enhanced edge detection using Laplacian Gaussian filtering method from different denoising images," *International Journal of Intelligent Systems and Applied Engineering*, vol. 12, no. 18s, pp. 313–323, 2024.

[65] R. Y. Yan and D.-Q. Zhang, "Edge detection based on channel attention and inter-region independence test," *arXiv preprint arXiv:2505.01040*, 2025.

[66] V. Maksimović, B. Jaksic, M. Milosevic, J. Todorovic, and L. Mosurovic, "Comparative analysis of edge detection operators using a threshold estimation approach on medical noisy images with different complexities," *Sensors*, vol. 25, no. 1, p. 87, 2024.

[67] R. Tang, S. Guo, K. Wang, H. Lin, L. Huang, and G. Mou, "A framework of insole blanking robot based on adaptive edge detection and FSPS-BIT* path planning," *Scientific Reports*, vol. 14, no. 1, p. 20791, 2024.

[68] G. Hu, "A mathematical survey of image deep edge detection algorithms: From convolution to attention," *Mathematics*, vol. 13, no. 15, p. 2464, 2025.

[69] H. Wang, P. Liu, Q. Dou, Y. Song, M. Luo, R. Han, and B. Zhang, "Enhanced edge detection via dual-branch attention fusion with Canny-assisted supervision: H. Wang et al.," *The Visual Computer*, pp. 1–16, 2025.